Journal of Environmental Chemical Engineering 12 (2024) 113630

Contents lists available at ScienceDirect

Journal of Environmental Chemical Engineering

journal homepage: www.elsevier.com/locate/jece

Synthesis of metal-free heteroatom (N, P, O, and B) doped biochar catalysts for enhanced catalytic co-pyrolysis of walnut shells and palm oil fatty acid distillate to produce high-quality bio-oil

Premchand Premchand [a,b,d], Debora Fino [b], Francesca Demichelis [b], Samir Bensaid [b], David Chiaramonti [c], George O'Connell [e], Jason Scott [e], Elsa Antunes [a,*]

[a] College of Science and Engineering, James Cook University, Townsville, Australia
[b] Department of Applied Science and Technology, Politecnico di Torino, Corso Duca Degli Abruzzi 24, Turin (TO) 10129, Italy
[c] Department of Energy, Politecnico di Torino, Corso Duca Degli Abruzzi 24, Turin (TO) 10129, Italy
[d] Department of Science, Technology and Society, University School for Advanced studies IUSS Pavia, Pavia (PV) 27100, Italy
[e] School of Chemical Engineering, The University of New South Wales, Sydney, UNSW 2052, Australia

ARTICLE INFO

Keywords:
Biomass
Catalytic co-pyrolysis
Heteroatom-doped biochar
Bio-oil upgrading
Aromatic hydrocarbons

ABSTRACT

In the current study, sugarcane bagasse-derived biochar catalysts were synthesized by doping with metal-free heteroatoms including nitrogen, phosphorus, oxygen, and boron and their efficacy was tested for catalytic co-pyrolysis of walnut shells (WS) and palm oil fatty acid distillate (PFAD) using Py-GC/MS. The biochar catalysts' properties and their effectiveness on co-pyrolytic bio-oil (overall product distribution, selectivity towards aliphatic and aromatic hydrocarbons, and carbon number ranges) were extensively examined. Among the various catalysts considered, boron-doped biochar (BCB) demonstrated effective performance due to an improved surface area, porosity, and acidity and resulted in a significantly increased hydrocarbon yield, particularly in the gasoline and diesel range, and preference for aromatic over aliphatic hydrocarbons. The optimum bio-oil quality was achieved at a feedstock-to-catalyst ratio of 2:1 and a pyrolysis temperature of 750 °C, with a hydrocarbon yield of 90.8 % and aromatic hydrocarbon selectivity of 63.5 %. Overall, the study underscores the role of BCB in fostering deoxygenation, decarboxylation, and aromatic selectivity via thermal and catalytic pathways, highlighting the potential of non-metallic doped biochars for bio-oil upgrading.

1. Introduction

The development of renewable energy resources has led to extensive research into innovative technologies capable of harnessing the enormous potential of feedstocks derived from biomass [1]. One of the most effective ways to produce biofuels from biomass is through pyrolysis, a thermochemical process that converts biomass into useful bio-oil, char, and gases [2,3]. However, because of its high oxygenated compound content, the resulting bio-oil often exhibits poor quality, being characterized by high viscosity, low thermal stability, and corrosiveness [4]. Thus, improving the quality of bio-oil is critical to its widespread use and economic viability [5]. Using catalysis is an important approach for improving bio-oil quality and increasing pyrolysis efficiency [6]. Yet, conventional catalysts, such as zeolites, have the disadvantage of being expensive and easily deactivated [7,8]. Therefore, biochar, which is a pyrogenic product of biomass, can be used as a heterogeneous, renewable, inexpensive, and efficient carbon-based catalyst in pyrolysis to reduce costs and prevent carbon deposition [9,10]. Biochar can be produced from all types of agricultural wastes [11] and its significant catalytic abilities are attributed to its tunable surface chemistry, porous structure, and surface functional groups [12,13]. Moreover, biochar's utilization as a catalyst is consistent with the ideals of eco-friendly and sustainable processes, which encourages further research into a wide range of applications [10,14]. Biochar can act as a channel for bio-oil's production enriched with valuable hydrocarbons via catalytic pyrolysis, paving the way for improved biofuel production and a lower environmental footprint [11,15].

Aside from using pristine biochar, a variety of modification strategies have been established to further improve its catalytic characteristics, such as physical and chemical activation, as well as metal and non-metal

* Corresponding author.
E-mail address: elsa.antunes1@jcu.edu.au (E. Antunes).

https://doi.org/10.1016/j.jece.2024.113630
Received 16 May 2024; Received in revised form 8 July 2024; Accepted 19 July 2024
Available online 20 July 2024

heteroatom doping [10]. In the literature, biochar [16], activated biochar [17,18] and metal-modified biochar [19–21] catalysts have been largely investigated for catalytic pyrolysis of various feedstocks to increase hydrocarbons content and lower the oxygen species in bio-oil. Among these, biochar modified with metals (Ni, Fe, Zn, Zr, Cu) showed the highest yield and selectivity for hydrocarbons [22,23].

Although metal- or metal oxide-modified biochar has shown exceptional selectivity and yield towards hydrocarbons, there are substantial limitations to utilizing metals such as leaching difficulties, poisoning, and cost [24]. Consequently, the focus has recently shifted to non-metal heteroatom doping, which involves chemically incorporating metal-free heteroatoms such as phosphorus (P), oxygen (O), nitrogen (N), and boron (B) into biochar, and can alter the catalyst surface structure and impact the yield and selectivity of the pyrolysis products [25]. For example, Chen et al., [26] investigated the influence of N doping on bio-oil composition produced during the catalytic pyrolysis of bamboo and discovered that the N-doped biochar catalyst significantly increased phenol generation up to (82 %). In contrast, doping P into biochar using phosphoric acid resulted in aromatic hydrocarbons being produced instead of phenol in the presence of a hydrogen donor (soap stick) [27]. The results are consistent with Su et al., [28] who reduced the oxygenates and nitrogenates content in bio-oil by 88.8 % and 83.2 %, respectively, from the catalytic co-pyrolysis of waste cooking oil and microalgae using P-doped biochar catalyst. The presence of functional groups in biochar is essential for its catalytic activity, thus an increase in the number of these groups can accelerate the reaction rate [29].

Despite growing interest, research on the effects of non-metal heteroatom doping in biochar on bio-oil compositions during pyrolysis has been limited to a few studies of N and P doping. Further examination of the effects of N and P doping, as well as additional heteroatoms such as B and O, on different feedstocks is needed, especially given the untapped potential of boron and oxygen heteroatoms. Incorporating these elements has the potential to introduce more active sites within the biochar, which could potentially alter the pyrolysis pathways. To the best of the author's knowledge there is no study available on the effects of B and O doping on the compositions of bio-oils. Consequently, the current study investigates the effects of N, P, O, and B doping on the catalytic properties of biochar produced from sugarcane bagasse (SCB) and the effectiveness of the synthesized catalysts for the co-pyrolysis of walnut shells (WS) and palm oil fatty acid distillate (PFAD) using Pyro/GC-MS. These three biomasses were chosen for the experiments due to their importance as industrial and agricultural byproducts, as well as their abundance. SCB is one of the most common agricultural wastes in the world [30] and walnuts are among the top four dried fruits consumed globally [31]. PFAD, a free fatty acid waste derived from industrial processes, has the potential to significantly increase hydrocarbon production during co-pyrolysis due to its higher hydrogen contents [32].

Initially a comparative analysis was conducted using five catalysts: (i) pristine biochar (BC); (ii) boron-doped biochar (BCB); (iii) phosphorus-doped biochar (BCP); (iv) nitrogen-doped biochar (BCN); and (v) oxygen-doped biochar (BCO), at a fixed pyrolysis temperature (650 °C). Subsequently, BCB was selected for optimization by varying temperature (550, 650, and 750 °C) and feedstock-catalyst ratio (1:1, 2:1, 4:1). This is the first comprehensive and comparative investigation of N, P, O, and B doping on biochar for the pyrolysis of walnut shells (WS) and palm oil fatty acid distillate (PFAD) by using first time PFAD as a unique hydrogen donor for catalytic co-pyrolysis.

2. Materials and methods

2.1. Materials

Three biomasses were used in this study: (i) Palm fatty acid distillate (PFAD) provided by the Malaysian oil palm industry; (ii) walnut shells collected locally; and (iii) sugarcane bagasse (SCB) obtained from Wilmar's Victoria Mill, Australia. All analytical-grade chemicals were purchased from Sigma-Aldrich, including oxalic acid (98 % purity), boric acid (99.5 % purity), orthophosphoric acid (85 % purity), and urea (99.0 % purity).

2.2. Biochar catalyst synthesis

The biochar catalysts were produced from SCB biomass. The SCB was thoroughly washed with distilled water to remove contaminants and then dried in an oven for 24 hours at 105 °C. For doping, the wet impregnation method was employed to incorporate four dopants (boric acid, oxalic acid, urea, and phosphoric acid) using a fixed ratio of 1:1 (SCB: dopants) based on previous studies [29,33,34] with some modifications. Briefly 4 g of SCB and 4 g of the selected dopant were mixed in 150 mL of distilled water and stirred continuously for 24 hours at 300 rpm with a magnetic stirrer. After impregnation, the water was separated by centrifugation and the biomass was dried in an oven for 24 hours at 105°C. The doped biomasses were then pyrolyzed in a horizontal quartz tube furnace at 600 °C (15 °C/min) for one hour under a N_2 atmosphere (2 L/min). Following pyrolysis, the biochars were washed twice with distilled water to remove unreacted dopants, then dried in an oven. To ensure reproducibility, each experiment was repeated at least three times. Biochar doped with boric acid, phosphoric acid, oxalic acid, and urea is labeled as BCB, BCP, BCO and BCN, respectively. The schematic overview of the procedure is depicted in Fig. 1.

2.3. Feedstock and catalyst characterizations

The feedstocks and biochar catalysts were characterized by thermogravimetric analysis (TGA), proximate and elemental analysis, nitrogen adsorption-desorption analysis, Field emission scanning electron microscopy (FE-SEM/EDS), Ammonia temperature programmed desorption (NH_3-TPD) analysis and Fourier-transform infrared spectroscopy (FTIR) analysis and X-ray photoelectron spectroscopy (XPS) analysis. The details of each characterization analysis are provided in Supplementary materials **(Text S1)**.

2.4. Pyrolysis GC/MS

The pyrolysis GC-MS experiments were carried out on a Shimadzu GCMS-QP2020 NX connected to a Multi-shot Pyrolyzer (EGA/PY-3030D). For catalytic co-pyrolysis, WS and PFAD feedstocks were used with a mixing ratio of 1:1 for all experiments. The samples were pyrolyzed at predetermined temperatures of 550, 650, or 750 °C for 1 min using N_2 carrier gas according to the previous studies [35] and helium gas was used to sweep pyrolysis vapors from the quartz furnace tube into the gas chromatograph mass spectrometer. For GC/MS, the injector temperature was set at 280 °C with a split ratio of 40:1. Product separation was achieved using a HP-5MS column with ultra-pure helium (99.999 %) at a flow rate of 1.0 mL/min. Peaks identification was performed by checking against the NIST library database and literature sources. Compounds with a similarity index above 75 % were used for analysis. The chromatographic peak area percentages were used to quantify the pyrolysis products. Before each analysis, blank runs were conducted until no identifiable peaks were observed. The relative selectivity of aromatic and aliphatic hydrocarbons, as well as the carbon numbers, was calculated by using Eq. (1) adopted from [36].

$$\text{Selectivity}\ (\%) = \frac{\text{Relative area \% of individual component}}{\text{Relative area \% of total hydrocarbons}} \times 100 \quad (1)$$

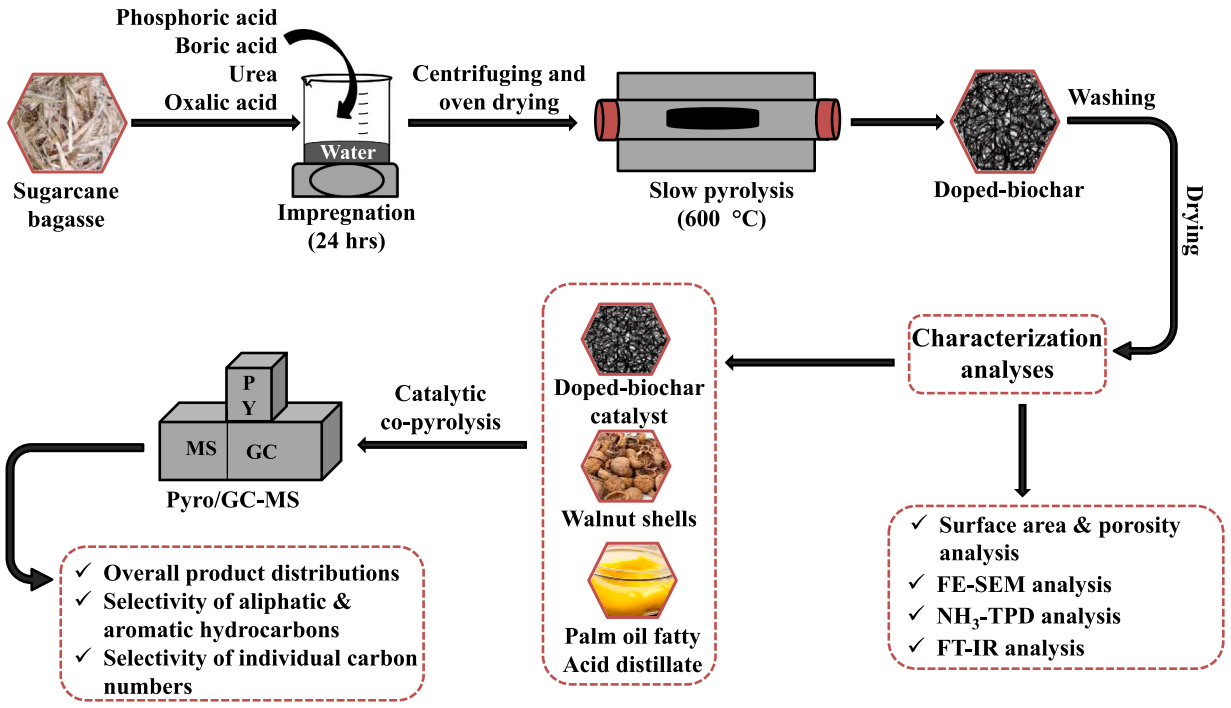

Fig. 1. Schematic overview of the procedure (materials and methodologies).

3. Results and discussion

3.1. Feedstock characteristics

The proximate and elemental compositions of feedstocks are listed in Table 1 and TGA analyses are depicted in Fig. 2. The SCB had a moisture content of 7.4 % and an ash content of 5.3 %, indicating the presence of minerals that could influence catalysis during pyrolysis [30]. Moreover, it showed 64.0 % volatile matter and 23.2 % fixed carbon content, useful for biochar production. In contrast, WS showed a lower fixed carbon content (16.8 %) and ash contents while higher volatile matter (72.8 %), indicating minimal inorganic interference and higher volatile product yields during pyrolysis [31]. On the other hand, unlike lignocellulosic biomass, PFAD was entirely composed of volatile matter (100 %), which was expected to behave differently during pyrolysis and completely breakdown when heated.

In terms of elemental composition, PFAD showed the highest percentage of carbon (74.9 %) and hydrogen (11.5 %) in comparison with SCB (42.5 % carbon, 4.9 % hydrogen) and WS (47.0 % carbon, 5.5 % hydrogen), which may potentially result in a higher energy content in the bio-oil [32]. The SCB, on the other hand, contained the highest oxygen (57.7 %), followed by WS (45.3 %) and PFAD (13.5 %), respectively.

Table 1
Proximate and elemental compositions of feedstocks: sugarcane bagasse (SCB), walnut shells (WS), and palm oil fatty acid distillate (PFAD).

	SCB	WS	PFAD
[a]Proximate analysis (wt%)			
Moisture	7.44	8.14	0
Ash	5.29	2.21	0
Volatile matter	64.02	72.82	100
[b]Fixed carbon	23.25	16.83	0
[a]Elemental analysis (wt%)			
Carbon	42.58	47.0	74.89
Hydrogen	4.99	5.52	11.55
Nitrogen	N/D	N/D	N/D
Sulphur	N/D	N/D	N/D
[b]Oxygen	47.14	45.27	13.56

[a] Dry basis
[b] Calculated by difference; N/D not detected

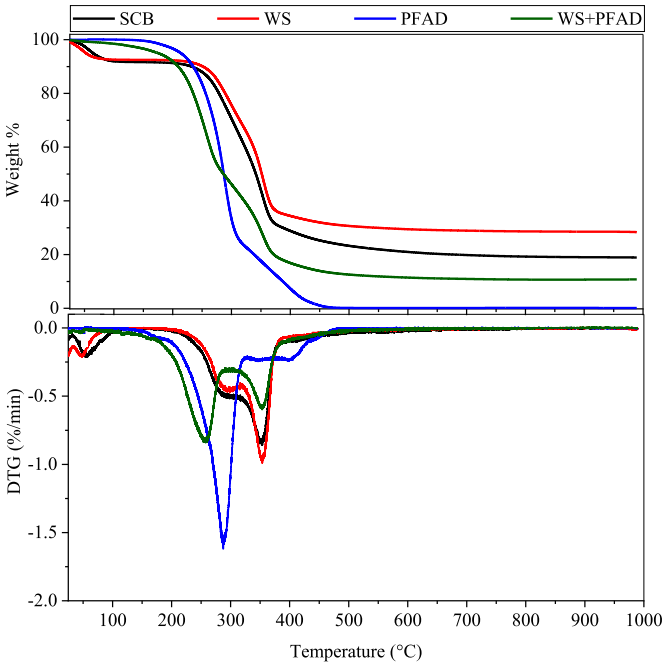

Fig. 2. TGA and DTG curves of biomass feedstocks sugarcane bagasse (SCB), walnut shells (WS), palm oil fatty acid distillate (PFAD), and mixture of SCB and WS.

Thermogravimetric analyses (Fig. 2) for WS and SCB demonstrated identical weight loss patterns and thermal stability, with notable decomposition occurred above 300 °C representing cellulose decomposition [37]. Compared to SCB, the WS lost weight more gradually, likely due to its higher lignin content which decomposes at higher temperatures [38].

Conversely, PFAD showed a noticeable and more pronounced weight

reduction at lower temperatures due to the higher volatility of fatty acids. Furthermore, the thermal behavior showed intermediate thermal stability between the individual components when WS and PFAD were blended (1:1) possibly due to the WS's fibrous structure interacting with PFAD's fatty components.

3.2. Production and characterizations of biochar catalysts

3.2.1. Biochar yield

The biochar yields from slow pyrolysis of SCB and SCB treated with urea, phosphoric acid, oxalic acid, and boric acid are shown in Table 2. The biochar yield from SCB was 26.1 wt% which was comparable with previous studies [39,40]. However, the addition of phosphoric acid and boric acid significantly increased the yield of biochar by approximately 73.9 % and 49.3 %, respectively. In contrast, adding oxalic acid and urea led to a substantial decrease in biochar yield by approximately 18.1 % and 13.3 %, respectively. The possible explanations for the observed changes in biochar yield are provided in Supplementary Materials **(Text S2).**

3.2.2. Biochar catalyst characteristics

The N_2 adsorption-desorption isotherms for the biochar catalysts are provided in Fig. S1 (Supplementary Materials) while the textural characteristics and SEM morphologies are presented in Table 3, and Fig. 3, respectively.

Compared to pristine BC, BCO exhibited a higher surface area of 388.0 m^2/g than BC (315.9 m^2/g). Additionally, BCO showed a larger total pore volume (0.234 cm^3/g), particularly in the mesopore range, implying that oxalic acid treatment effectively expanded pore channels. This was further supported by SEM observation (Fig. 3), which showed that BCO had a more rugged and porous structure with clear pore widening compared to BC's smoother morphology. Thus, oxalic acid modification has the capacity to enhance BCO's catalytic potential such as increased surface area and mesoporosity, which could promote better reactant accessibility [4].

When examining the impact of nitrogen doping, urea impregnation had a significant effect on biochar's textural properties. Both BC and BCN isotherms exhibited Type I characteristics (Fig. S1), which are typical of microporous materials [36].

Compared to BC, BCN exhibited a lower surface area (232.2 m^3/g) than BC (315.9 m^2/g). This finding implies that urea impregnation may have caused partial micropore blockage or narrowing, reducing the average pore diameter and total pore volume [41]. The mesopore volume remained unchanged, indicating that nitrogen doping mostly impacted the microstructure rather than the mesoporous framework, which could have implications for catalytic applications requiring micropore accessibility [42].

The phosphorus doped biochar (BCP) resulted in significant changes in its porous properties. Phosphorus incorporation significantly reduced the BET surface area for BCP from 315.9 m^2/g (BC) to 81.8 m^2/g (BCP). Moreover, BCP also demonstrated a lower total pore volume compared to BC, indicating that phosphoric acid treatment led to pore contraction or closure. The micropore volume also decreased from 0.100 cm^3/g (BC) to 0.022 cm^3/g (BCP), indicating further pore narrowing. This suggests that the biochar structure was densified, reducing its ability to adsorb the same amount of nitrogen. The SEM images further confirmed that BCP had a smoother surface with fewer pores than BC's open porous network, as evident in Table 3. Thus, phosphorus doping resulted in a denser biochar with reduced porosity which could affect its performance in applications where pore volume and surface area are critical parameters. Literature studies [28,43] showed that phosphoric acid impregnation always increased surface area and porosity due to H_3PO_4 acting as an effective activating agent to generate pore structure. However, opposite findings observed in the current study could be due to possible over-concentration of phosphoric acid resulted in pore-congestion and/or specific interactions between the phosphorus compounds and the carbon matrix that hindered pore formation.

Table 2
The effect of heteroatom doping on biochar yield produced from the slow pyrolysis of sugarcane bagasse at 600 °C.

No.	Feedstock	Heteroatom	Precursor	Biochar yield (wt%)
1	SCB	/	/	26.12 ± 2.12
2	SCB	Phosphorus	Phosphoric acid	45.37 ±1.71
3	SCB	Boron	Boric acid	38.95 ± 0.08
4	SCB	Oxygen	Oxalic acid	21.39 ± 0.40
5	SCB	Nitrogen	Urea	22.64 ± 1.03

Table 3
Surface area and porosity characteristics of biochar catalysts produced from the slow pyrolysis of SCB impregnated with different precursors. Ratio of SCB to precursor = 1:1.

Sample	[a]BET surface area (m^2/g)	[b]Total pore volume (cm^3/g)	[c]Micropore volume (cm^3/g)	[d]Mesopore volume (cm^3/g)	[f]Average pore diameter (nm)
BC	315.9	0.193	0.100	0.093	3.18
BCO	388.0	0.234	0.118	0.116	3.92
BCN	232.2	0.161	0.065	0.096	3.06
BCP	81.8	0.064	0.022	0.042	2.01
BCB	431.5	0.204	0.151	0.053	3.98

[a] BET method;
[b] single point at P/Po=0.99;
[c] t-plot method;
[d] Vmeso= Vtotal -Vmicro;
[f] BJH desorption

Boron doping substantially enhanced the textural properties of biochar (BCB). For example, the BET surface area of BCB increased from 315.9 m^2/g (BC) to 431.5 m^2/g. Additionally, BCB showed a significant increase in meso- and microporous structures, with a total pore volume of 0.204 cm^3/g which was in-line with previous studies [29,44]. These changes were further confirmed by SEM images, which revealed that the morphology of BCB consisted of a variety of distinct, well-defined, and connected pores, compared to BC's more compact and less porous structure, as evidenced by pore volume and isotherm measurements. The improvement in textural properties was thought to be due to boric acid's catalytic effect on the dehydration and depolymerization reactions of biochar, which accelerated the removal of volatile organic matter from biomass materials during pyrolysis [29,44]. The boron doping process appeared to increase the size of existing pores while also creating new ones, which can significantly improve the material's potential as a catalyst by increasing its active surface area facilitating reactant diffusion through the pores to the active sites.

The NH_3 TPD analysis for the different doped biochars provided information on their surface acidity. As depicted in Fig. 4, pristine biochar (BC) had a moderate desorption peak that served as a starting point for comparing acidity.

The highest desorption intensity was seen in boron-doped biochar (BCB), particularly at higher temperatures, suggesting the formation of borate or boron-oxygen groups that caused the significant increase in strong acid sites [45]. A desorption peak at lower temperatures was observed for BCN, indicating the presence of weak acid sites that may have originated from nitrogen-containing groups such as amines or amides [46]. For BCO, an increased desorption peak intensity at intermediate temperatures was observed indicating a greater number of medium-strength acid sites, most likely from oxygen functionalities like carboxylic groups. Finally, BCP exhibited two distinct desorption peaks, indicating a complex acid profile with weak and strong acid sites that may have originated from phosphate groups [47].

The FT-IR spectra of pristine biochar (BC) and heteroatom-doped biochars (BCN, BCO, BCP and BCB) are provided in Fig. 5. The FT-IR

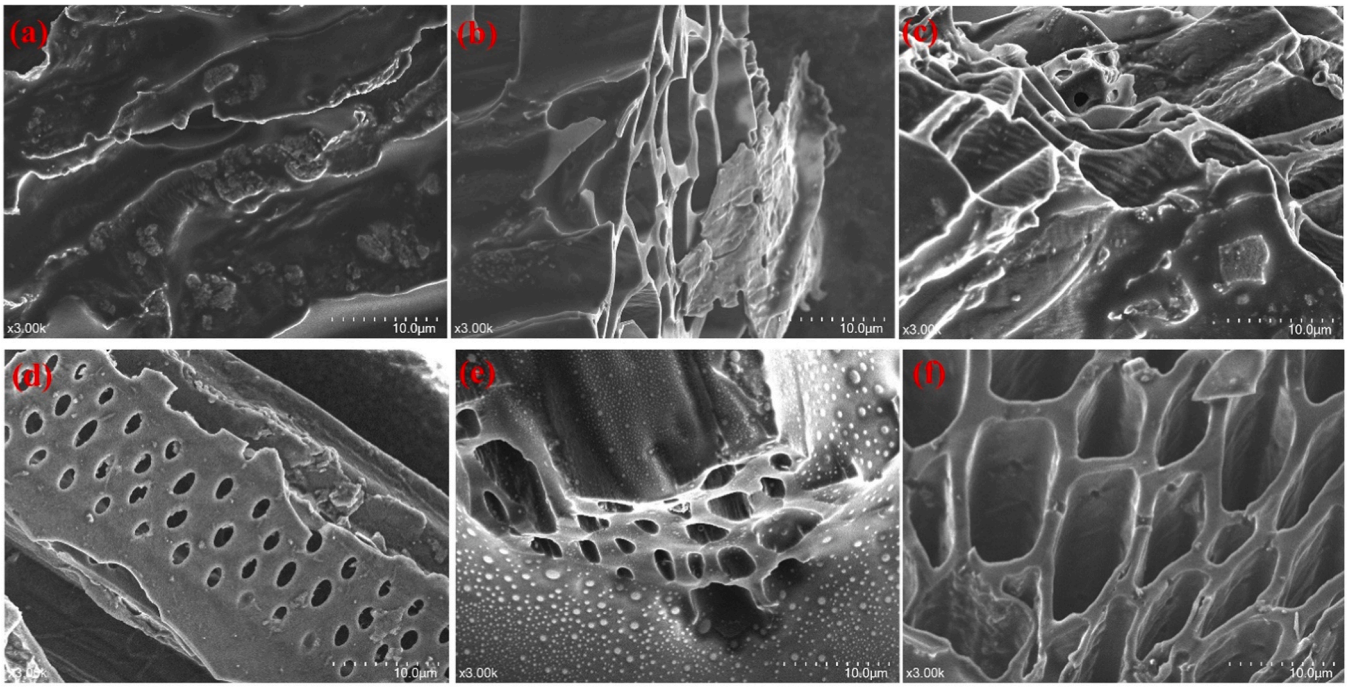

Fig. 3. SEM images of SCB (a), BC (b), BCO (c), BCN (d), BCP (e), and BCB (f) at 10.00 μm scale x3.00 k.

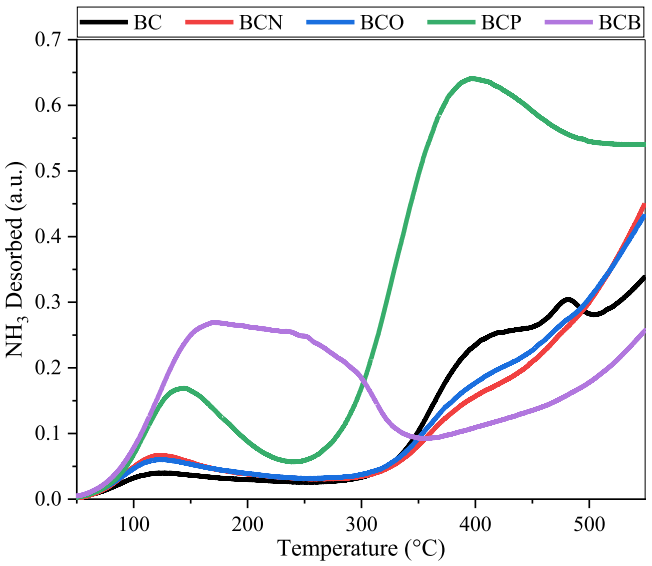

Fig. 4. NH_3 TPD profiles of biochar catalysts (BC, BCN, BCB, BCO, and BCP).

spectrum of BC showed several distinct peaks, including a weaker broad band around 3400 cm^{-1}, indicating the presence of -OH groups [1], and a peak near 1600 cm^{-1}, indicating aromatic structures and C═C stretching vibrations [48]. The sharp peak at around 1000 cm^{-1} was attributed to the stretching of the C-OH, C-O, and C-O-C functional groups [49]. Nitrogen doping invoked the formation of nitrogen functionalities by increasing intensity and forming new peaks for BCN. A new peak at around 3430 cm^{-1} was attributed to N-H stretching [50], while sharper and more intense peaks at 1630 cm^{-1} could be due to C═N and N-H bending vibrations, indicating amine or amide functionalities [51].

Oxygen doping was evident by the widening and intensification of peaks corresponding to oxygen-containing groups. The sharp peak at 1735 cm^{-1} indicated C═O stretching from carboxylic acids [24], whereas the strong peak at 1030 cm^{-1} could be due to C-O stretching in ethers or esters [52]. Phosphorus doping was confirmed by the formation of new peaks and intensity shifts in the BCP spectrum. Specifically, the peak at 1030 cm^{-1} could be attributed to P-O-C stretching vibrations, which indicates the formation of phosphate esters or organophosphates [53]. In addition, the peak at 560 cm^{-1} was attributed to P-O-Phosphate stretching vibrations.

The introduction of boron was observed in changes at lower wavenumbers in the BCB spectra. The peak at 1390 cm^{-1} was attributed to B-O stretching [44] and the subtle features at around 700–800 cm^{-1} suggested B-O-B bending vibrations, indicating boron incorporation into the biochar's lattice structure [24]. The BCB was further analyzed using XPS, TEM, and EDS to gain a better understanding of the surface composition and chemical states of the elements present. As shown in Fig. 6, the full survey spectrum revealed distinct peaks for C 1 s (284.2 eV), O 1 s (533.8 eV), N 1 s (400.5 eV), and B 1 s (191.9 eV), with 65.1 % of C, 25.9 % of O, 4.9 % of B, and 4.1 % of N, confirming successful boron doping and significant oxygen content, consistent with previous studies on boron doped biochars [29,54]. The high-resolution spectrum for C 1 s demonstrated numerous peaks, including C-C, sp^2 carbon at 284.7 eV, C-O at 285.2 eV, C═O at 286.2 eV, and O-C═O at 288.2 eV, indicating a variety of carbon structures, including graphitic, alcohols, ethers, carbonyls, and carboxylate groups [24,54].

Moreover, the peaks O-H, C-OH/C-OOH, and O-C/O-B-O were visible in the O 1 s spectrum at binding energies of 533.1, 533.5, and 533.8 eV, suggesting a variety of oxygen functionalities in the BCB, including the formation of hydroxyl and carboxyl groups and boron-oxygen bonds [24,29]. Lastly, The B 1's high resolution spectrum revealed two visible components: B_2O_3 at 193.8 eV, indicating strong boron inclusion into the carbon matrix; and BC_2O at 191.1 eV, suggesting surface oxidation [44]. The boron oxides resulting from the interaction between boric acid and biomass during pyrolysis can be represented using the following possible equations [29]:

$$2B\ (OH_3) \rightarrow B_2O_3 + 3H_2O \quad (2)$$

$$B_2O_3 + 6C \rightarrow BC_3 + BCO_2 + B\ C_2O \quad (3)$$

Moreover, the microstructure of the BCB was examined in detail by

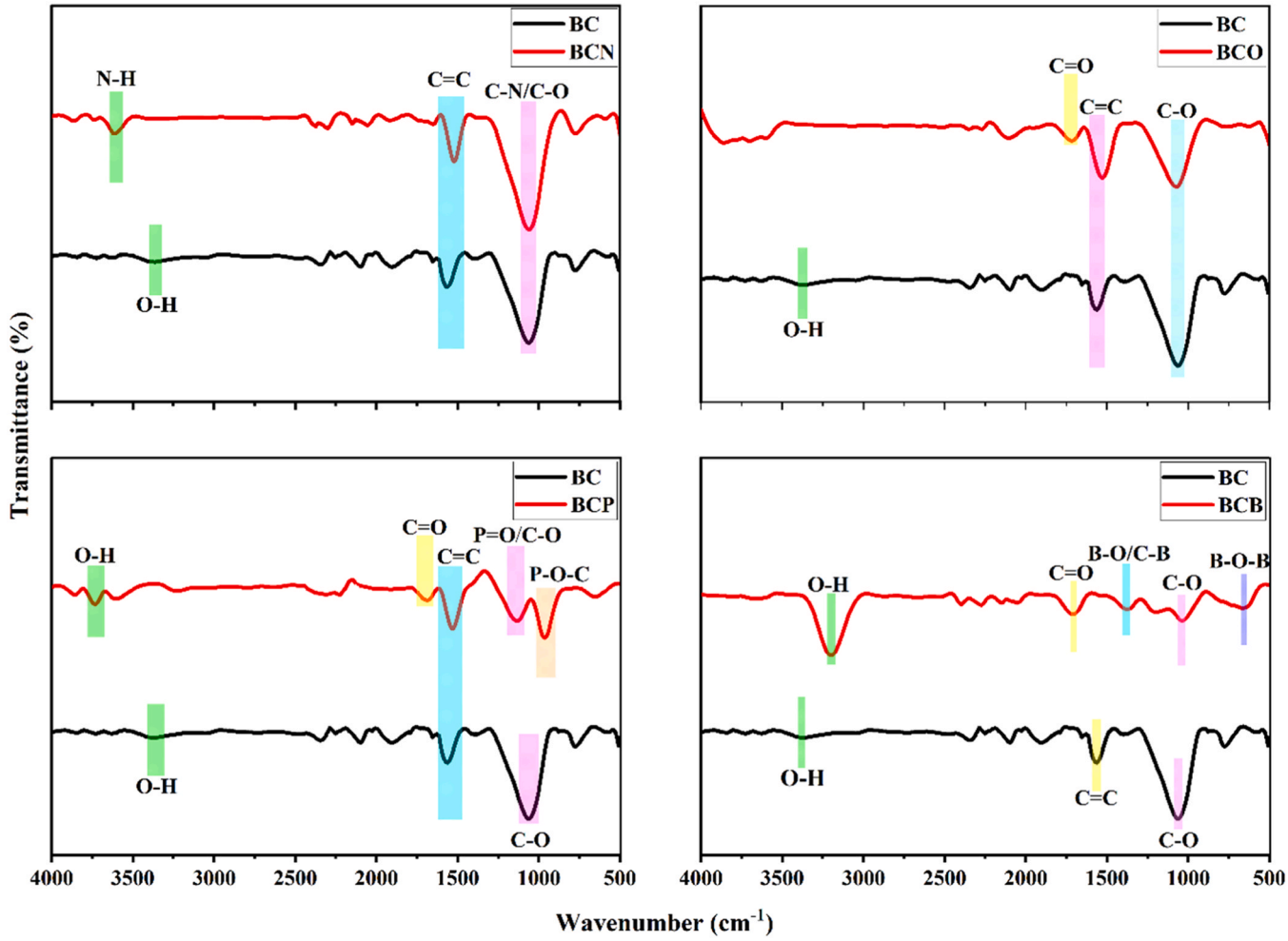

Fig. 5. FT-IR spectra of pristine biochar (BC) and biochar-doped with nitrogen (BCN), phosphorus (BCP), oxygen (BCO), and boron (BCB).

the TEM analysis (Figure S3), which revealed amorphous carbon regions, thin film collections, and a solid amorphous matrix with inclusions. These findings suggested that boron doping had a major effect on the structural properties of the BCB, which was consistent with the previous study [54].

The EDS spectrum (Figure S4) indicated that BCB was primarily composed of carbon, with a notable oxygen content and trace amounts of silicon impurities. It is worthwhile to mention that boron was not detected in EDS; this could be due to the boron's lower atomic number, ionization concerns, and low fluorescence yield upon exciting, making it difficult to detect [55].

3.3. Pyrolysis product characteristics

3.3.1. Non-catalytic pyrolysis of WS and PFAD

The overall product distributions, selectivity of aliphatic and aromatic hydrocarbons, and selectivity of carbon number range arising from the non-catalytic pyrolysis of WS, PFAD, and co-pyrolysis of WS and PFAD at 650 °C are shown in Fig. 7.

The primary organic compounds in bio-oil were classified into eight categories based on their chemical structures, which include hydrocarbons, phenols, ketones, aldehydes, alcohols, acids, esters, and furans. As depicted in Fig. 7 **(a)**, the major products from WS pyrolysis were hydrocarbons (28.1 %), phenols (21.0 %), ketones (15.7 %), acids (14.6 %) and aldehydes (14.3 %) as well as a lower proportion of alcohols and furans (4.4 %), which were reasonably comparable to prior studies on WS [35,56,57]. A significant amount of aliphatic hydrocarbons was also present indicating that the extractives (>10 %) found in walnut shells, such as oils, waxes, and fats, could be the main reason for higher hydrocarbons [31,58].

Considering the selectivity of aliphatic and aromatic hydrocarbons, as previously stated, WS bio-oil predominately contained aliphatic hydrocarbons (22.5 % yield) with 80 % selectivity, as shown in Fig. 7 **(b)**. The selectivity of individual carbon number contents in bio-oil is depicted in Fig. 7 **(b)**. Carbon numbers can be divided into two categories: gasoline (C5-C11) and diesel (C12-C20) [23,59]. The WS bio-oil contained 85.9 % gasoline range hydrocarbons and 14.4 % diesel range hydrocarbons. C8 hydrocarbons were dominant in the gasoline range followed by C6, while C12 hydrocarbons were dominant in the diesel range followed by C14 (Table S1).

On the other hand, PFAD bio-oil contained the highest concentration of hydrocarbons (63.9 %), followed by acids (27.7 %), and a small proportion of phenols, ketones, alcohols, and esters. Aliphatic hydrocarbons accounted for 97.0 % of total hydrocarbons dominated by alkenes (77 %) and alkanes (23 %) including 1-undecene (8.7 %), 1-octene (5.9 %), 1-heptene (5.8 %), tetradecane (5.3 %), 1-octane (4.3 %) and 1-tetradecene (4.5 %) as well as small proportions of other alkanes and alkenes. Malaysian PFAD is typically made up of free fatty acids, including saturated fatty acids consisting of palmitic acid (46 %), stearic acid (4.3 %), myristic acid (1.2 %) and lauric acid (0.4 %), as well as unsaturated fatty acids including oleic acid (36.7 %) and linoleic acid (9.0 %) [32]. The pyrolytic process involves complex cracking, decarboxylation and decarbonylation reactions of free fatty acids that results in a variety of long-chain alkanes and alkenes [60].

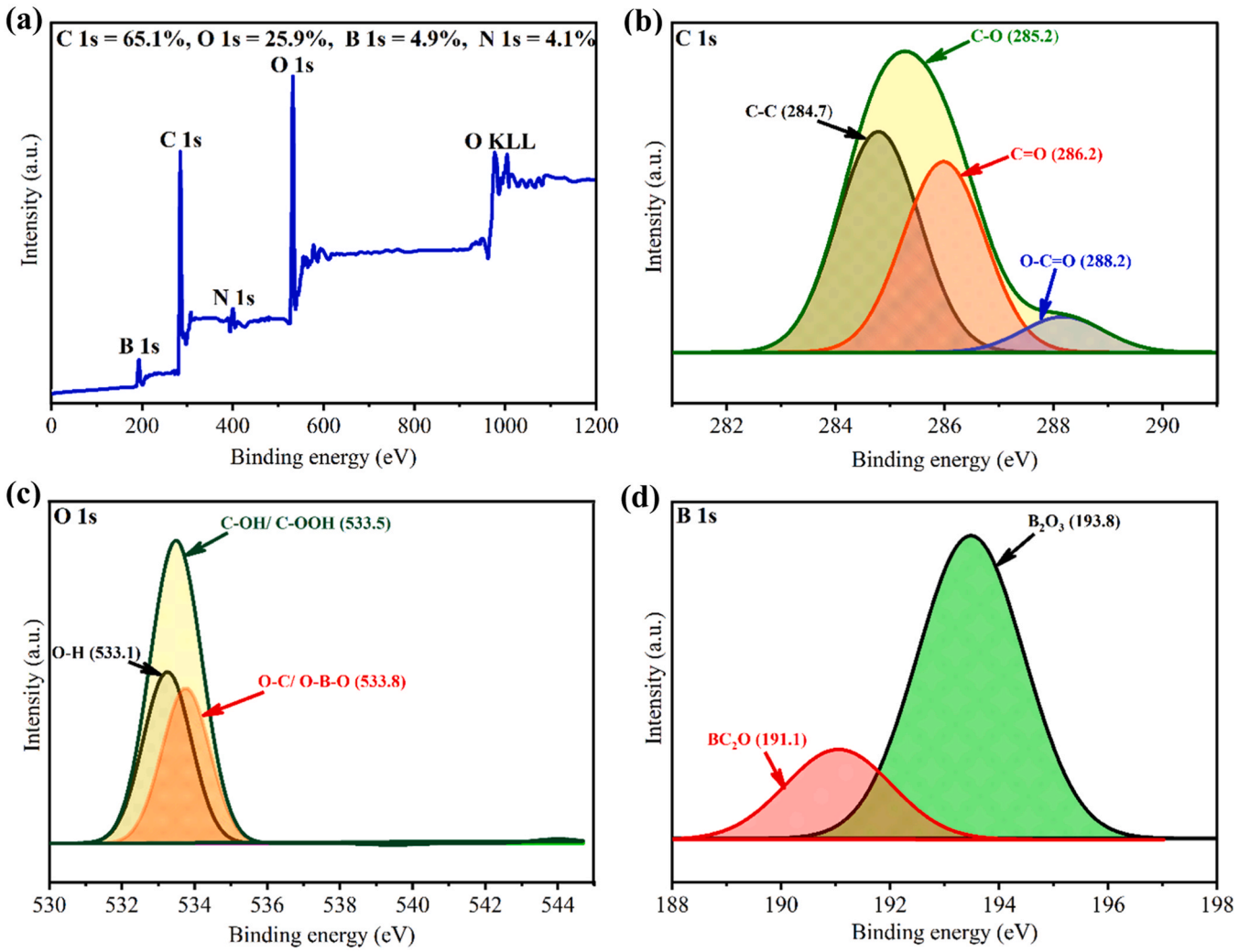

Fig. 6. XPS full spectra of BCB (a), high resolution spectra of C 1 s (b), O 1 s (c) and B 1 s (d).

1-undecene, 1-octene, 1-heptene, and 1-tetradecene were the major alkene compounds found in PFAD bio-oil. Fatty acid pyrolysis may have followed a free-radical chain reaction mechanism via β-scission, resulting in the breaking of C-C bonds and the significant production of small-molecule unsaturated hydrocarbons such as propene, 1-heptene, and 1-octene [61,62].

In the literature, no study is available that directly reported the fast pyrolysis/GC-MS of PFAD. However, there are a few studies available that reported the pyrolysis characteristics of individual fatty acids as a model component such as palmitic acid and oleic acid [63,64]. Furthermore, the acidic compounds in the PFAD bio-oil were palmitic acid (11 %) and oleic acid (6 %) which indicated that some of the PFAD components were partially decomposed.

When the WS and PFAD were co-pyrolyzed, the bio-oil contained the highest proportion of hydrocarbons (71.5 %), followed by acids (17.4 %). The hydrocarbon yield was higher than from individual WS and PFAD pyrolysis, which could be attributed to the distinct properties of the two feedstocks. PFAD aided in the production of aliphatic hydrocarbons due to their high fatty acid content, whereas WS's lignocellulosic components produced aromatic and aliphatic hydrocarbons during the pyrolysis process. Among the hydrocarbons, co-pyrolysis improved aromatic hydrocarbon selectivity (24.4 %), outperforming WS and PFAD pyrolysis alone (20.1 % and 2.9 %) as shown in Fig. 7 **(b)**. The primary aromatic compounds in the co-pyrolytic bio-oil were benzene, toluene, ethylbenzene, and p-xylene. This suggests that co-pyrolysis had a positive synergistic effect on aromatic hydrocarbons, with phenolic, ketonic, and aldehyde compounds from WS most likely being converted into aromatic hydrocarbons via different reaction pathways such as cyclization, deoxygenation, and aromatization [65].

In contrast, oxygenated compounds in the WS bio-oil were notably reduced suggesting that co-pyrolysis significantly reduced the oxygen in bio-oil. It is worth noting that the acid component (17.4 %) in the co-pyrolysis product contained only palmitic and oleic acid, which was likely to arise from PFAD. However, acetic acid in WS (14.6 %) was completely converted into hydrocarbons during co-pyrolysis. Examining the selectivity of carbon numbers, co-pyrolysis significantly enhanced the gasoline range carbon number to 90 % which was higher than the individual pyrolysis of WS (85.5 %) and PFAD (67.9 %). Overall, the synergistic effect of co-pyrolyzing WS and PFAD at 650 °C enhanced the bio-oil quality. While oxygenated compounds in WS were significantly reduced, the total hydrocarbon yield and selectivity towards aromatic hydrocarbons significantly increased, illustrating the potential of co-pyrolysis to improve bio-oil quality.

3.3.2. Catalytic co-pyrolysis of WS and PFAD

The ensuing section compares the effects of different biochar catalysts (BC, BCB, BCP, BCN, and BCO) on the co-pyrolysis of WS and PFAD (ratio 1:1). The pyrolysis/GC-MS experiments were conducted at 650 °C with a fixed feedstock-to-catalyst ratio (1:1) and results are shown in Fig. 8. Prior to choosing the pyrolysis temperature, the TGA analysis was

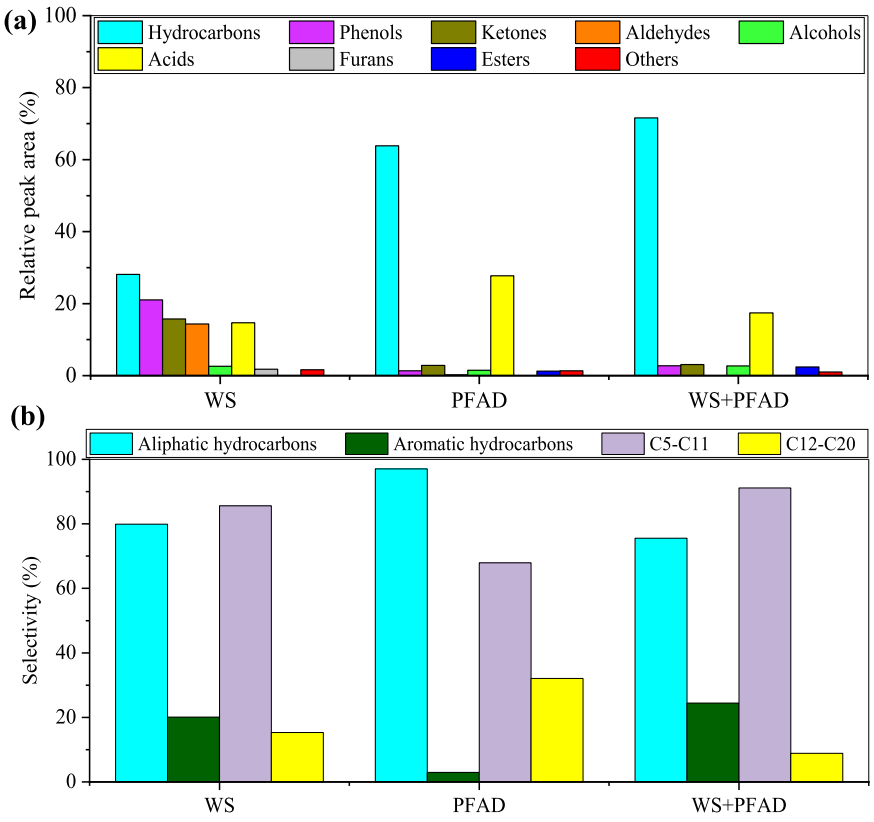

Fig. 7. Non-catalytic pyrolysis of WS, PFAD and co-pyrolysis of both WS and PFAD (a) overall product distribution and (b) selectivity towards aliphatic and aromatic hydrocarbons and selectivity of carbon number range.

performed to determine the thermal stability of the biochar. The results (Figure S2) indicated that the biochar was stable up to 800 °C and experienced only minor weight loss (about 3–4 %).

3.3.2.1. Effect of pristine biochar catalyst. The effect of BC as a catalyst on co-pyrolytic bio-oil production is shown in Fig. 8. As observed in Fig. 8 **(a)**, the distribution of products changed significantly upon biochar addition. Hydrocarbon production was improved by 5.1 %, increasing from 71.5 % to 75.2 %. A shift towards more aromatic ring structures was evident with the selectivity to aromatic hydrocarbons increasing by 16.3 % and aliphatic hydrocarbons decreasing by 6.3 % (Fig. 8 **(b)**). Among the hydrocarbons, toluene, p-xylene, o-xylene, and various benzene derivatives were the most abundant aromatics. The increase in these compounds upon BC addition indicates the shift was probably caused by enhanced cyclization and aromatization reactions on the surface of the biochar [16]. BC may have provided sites that assisted stabilization of the transition states that resulted in these compounds or facilitated the dehydrogenation and cyclization of aliphatics [7]. There was also a shift in selectivity for the carbon numbers, with longer chain hydrocarbons (C15–C20) increasing by a substantial 265.8 % and shorter chains (C5) decreasing by 41.9 % (Fig. 8 **(b)** and Table S1). The gasoline range hydrocarbons (C5-C11) decreased from 91.1 % (non-catalytic) to 83.6 % (catalytic), while diesel range hydrocarbons (C12-C20) increased from 8.8 % (non-catalytic) to 15.3 % (catalytic).

Conversely, the amount of phenol increased significantly (by 151.4 %), indicating that biochar had a strong catalytic effect on phenol formation. While the ketone concentration did not appreciably change, the amount of alcohol increased significantly (by 57.2 %). The acids produced decreased considerably from 17.4 % to 0.4 %, indicating that biochar was an effective catalyst for decarboxylation and decarbonylation reactions. In contrast, the ester content increased from 2.4 % to 5.9 %, possibly due to improved esterification processes enabled by the biochar's acidic sites. Based on the catalytic action of the biochar, there may be a correlation between the decrease in long-chain fatty acids, like palmitic and oleic acids, and the increase in phenols and esters contents. The fatty acids may have reacted more readily due to the double bond that exists between their carbon and carbon-oxygen atoms. Biochar could aid in the formation of rings in the acid structures as well as the removal of water. This may have triggered additional chemical reactions resulting in the creation of numerous aromatic compounds, including phenols [10]. In the literature (Table S2), studies [7,10,16] have reported a similar trend with slight variations on effects of using pristine biochar as a catalyst on bio-oil composition obtained from pyrolysis or co-pyrolysis of biomass, due to differences in feedstocks and pyrolysis conditions.

3.3.2.2. Effect of boron-doped biochar catalyst. Examining the effect of the BCB catalyst, compared to non-catalytic pyrolysis, BCB had a significant effect on the pyrolytic products. Hydrocarbons significantly increased from 71.5 % to 86.8 %, representing a 21.3 % increase in hydrocarbon yield. In terms of hydrocarbon compositions, the selectivity to aromatic hydrocarbons increased from 24.4 % to 36.7 % while the selectivity to aliphatic hydrocarbons decreased from 75.5 % to 63.2 %. The major aliphatic hydrocarbons found in the resulting bio-oil were 1,3-cyclopentadiene, 2-butene, 2-methyl-, 2-pentene, 2-methyl-, 4-methylenecyclopentene, heptadecane, cyclopentene, and 7-tetradecene while the main aromatics were p-xylene, 1,3-dimethyl-benzene, propyl-benzene, indane, 1,2-diethyl-benzene, and naphthalene. There was a significant shift in the carbon number distribution, with a considerable rise in C5 hydrocarbons and a general decline in higher carbon number hydrocarbons over the BCB catalyst. Additionally, when compared to non-catalytic pyrolysis, the gasoline range hydrocarbons (C5-C11) over BCB catalyst decreased from 91.1 % to 85.8 %, while the diesel range (C12-C20) hydrocarbons increased proportionally. The boron in BCB likely provided more catalytic sites for the pyrolysis

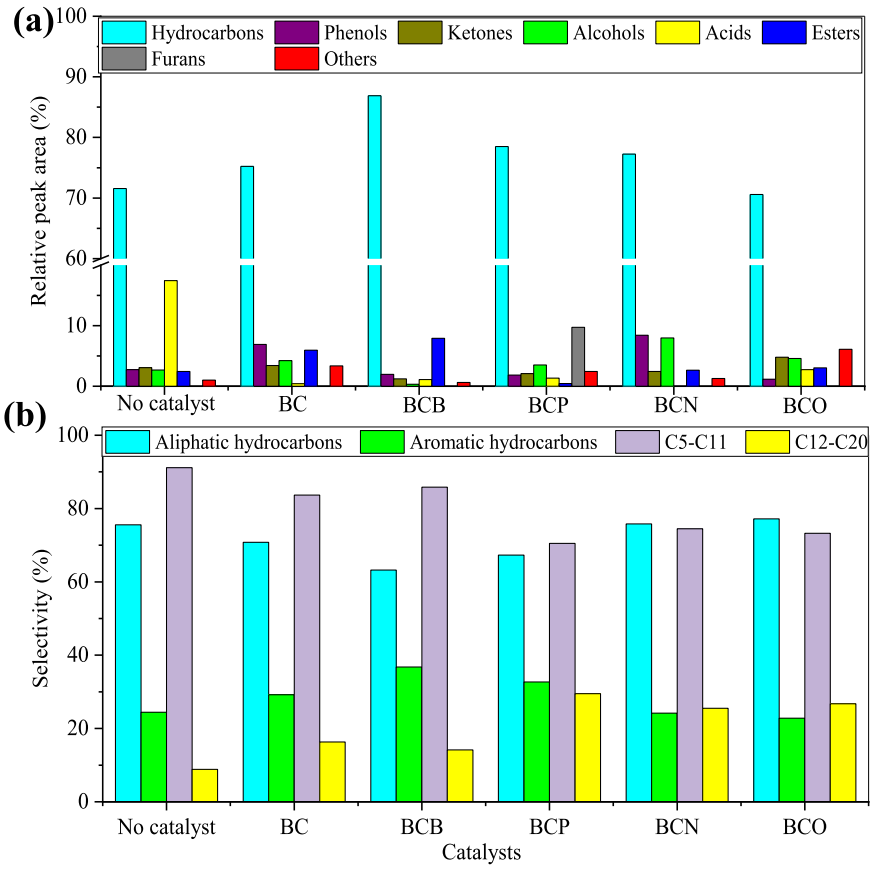

Fig. 8. Effect of biochar catalysts on (a) overall product distribution, and (b) selectivity towards aliphatic and aromatic hydrocarbons and selectivity of carbon number range from the co-pyrolysis of WS and PFAD (1:1 ratio).

process by facilitating the breaking down (cracking) of larger molecules into smaller hydrocarbon chains, as evidenced by the rise in C5 hydrocarbons. Furthermore, the formation of borate esters and the unique electronic structure of boron may have aided in the stabilization and rearrangement of reaction intermediates, increasing hydrocarbon production.

In contrast, the acid content decreased from 17.4 % to 1.1 % and ester content increased from 2.3 % to 7.9 %, representing a substantial increase of 225 %. The observed increase in ester content, particularly in the case of the hexanoic acid-pentadecyl ester, could be attributed to the esterification reactions catalyzed by BCB. In these reactions, alcohols found in the pyrolysis vapors could have reacted with fatty acids from PFAD (palmitic acid) to form esters [60].

There was also a substantial decrease in oxygenated functional groups such as alcohols (from 2.7 % to 0.3 %), phenols (from 2.7 % to 1.9 %), and ketones (from 3.1 % to 1.2 %). The reduction in phenols suggests that BCB may have promoted ring saturation and hydrogenation processes that converted them to hydrocarbons. The significant decrease in alcohols indicates that deoxygenation was taking place efficiently, which could occur through reactions such as dehydration to form alkenes, which can then be hydrogenated to form alkanes. Alternatively, the decrease in ketones could be due to BCB catalyzing deoxygenation reactions such as decarbonylation, which converted ketones to alkanes and possibly alkenes. There appeared to be no existing literature reporting the catalytic effect of boron-doped biochar on biomass pyrolysis, making the findings of this study novel. Overall, boron-doped biochar significantly altered the bio-oil composition in the catalytic pyrolysis of WS and PFAD, increasing the production of hydrocarbons while significantly lowering oxygenated species such as phenols, alcohols, ketones, and acids. The findings suggest that the unique properties of BCB influenced the pyrolysis reaction pathways and intermediates. BCB appeared to be a promising catalyst for upgrading bio-oil, due to its multifunctional role in deoxygenation, it can selectively convert pyrolysis intermediates into desired products.

3.3.2.3. Effect of phosphorus-doped biochar catalyst. Examining the effect of BCP on co-pyrolytic bio-oil production, as shown in Fig. 8 **(a)**, BCP also increased the total hydrocarbon yield from 71.6 % to 78.5 %. The enhancement suggested that the catalyst was beneficial for deoxygenation and carbon-carbon bond formation reactions [28]. Furthermore, the reduction in phenol content from 2.7 % to 1.8 % suggested that phosphorus may have aided in the demethoxylation and dehydration reactions that converted phenols to aromatic hydrocarbons [27]. Interestingly, a high percentage of furans (9.7 %) was also found in the BCP-derived bio-oil, indicating a shift toward more thermally stable aromatic structures [66]. In terms of selectivity, the addition of BCP significantly increased aromatic hydrocarbon selectivity from 24.4 % to 32.7 % while decreasing aliphatic hydrocarbon selectivity from 75.5 % to 67.3 % (Fig. 8 **(b)**). The introduction of polarity and acidic sites via phosphorus doping may have promoted cyclization and aromatization reactions, resulting in a higher aromatic yield. Moreover, there was a discernible rise in heavier hydrocarbons (C15–C20) from 3.5 % to 14.5 % over the BCP catalyst (Table S1). The formation of longer-chain hydrocarbons could be favored by the catalytic properties of BCP, which may have promoted oligomerization and chain growth reactions. In terms of gasoline and diesel range hydrocarbons, compared to the non-catalytic pyrolysis, the gasoline range hydrocarbons (C5-C11) decreased from 91.2 % to 77.6 % over the BCP catalyst, while the diesel range hydrocarbons increased from 6.4 % to 29.5 %. The major aliphatic hydrocarbons found in bio-oil were cyclopentene, 1-methyl-; 1-octene; 7-tetradecene; octadecane; 3-octadecene, (*E*)-; 1-butene, 3, 3-dimethyl- and many others whereas the main aromatic hydrocarbons

were toluene; p-xylene; benzene, and 1,3-diethyl-benzene. These findings were consistent with previous research [27,28], with some variations (Table S2) due to feedstock variability and different pyrolysis conditions. Overall, the BCP catalyst had a significant impact on co-pyrolysis by increasing aromatic hydrocarbon production and facilitating the formation of longer-chain, more complex hydrocarbons. The changes were attributed to the BCP's improved catalytic properties, which accelerated the reaction pathways of cyclization, aromatization, and oligomerization.

3.3.2.4. Effect of nitrogen-doped biochar catalyst. The catalytic effect of BCN on co-pyrolytic bio-oil generation is presented in Fig. 8. BCN increased the overall hydrocarbon yield from 71.6 % to 77.2 % implying that BCN accelerated the deoxygenation and carbon-carbon linking reactions. In terms of hydrocarbon selectivity, the addition of BCN had no major effect on the selectivity of aliphatic and aromatic hydrocarbons, as it was almost identical to that produced by non-catalytic pyrolysis. However, BCN provided a noticeable shift toward heavier hydrocarbons (C15-C20), increasing from 3.5 % to 9.5 % (Table S1). This can be attributed to the nitrogen in the biochar promoting condensation or polymerization reactions, which resulted in longer-chain hydrocarbons [67]. Furthermore, a significant increase in C5 hydrocarbons (from 11.8 % to 15.0 %) implied that nitrogen doping may have assisted the formation or stabilization of shorter carbon chains. In terms of gasoline and diesel range hydrocarbons, BCN significantly decreased the gasoline range hydrocarbons from 91.2 % to 79.4 %, while concurrently increasing the diesel range hydrocarbons from 6.4 % to 16.1 % (Fig. 8 **(b)**).

The phenol content increased substantially from 2.7 % to 8.4 %, implying that nitrogen functional groups in biochar aided in the formation of phenolic compounds, possibly through ammonia-driven processes that stabilized the phenol precursors [68]. A significant reduction in acids, from 17.4 % to 0 %, showed that BCN was effective for de-acidifying the process. On the other hand, the alcohol content tripled when the BCN catalyst was present, indicating a possible shift toward hydroxyl group-stabilized intermediates [41]. Other studies [67] have reported an increase in phenolic compounds during catalytic pyrolysis by nitrogen-doped biochar/activated carbon materials (Table S2). This was attributed to the introduced nitrogen active sites promoting deoxygenation, cracking, aromatization, and Diels-Alder reactions of the co-pyrolysis vapors [26]. Overall, the findings indicate that nitrogen-doped biochar had a significant impact on both the yield and the chemical nature of the hydrocarbons produced during co-pyrolysis. The BCN reaction mechanisms were most likely multifaceted, involving a combination of basic catalysis, reactive intermediate stabilization, hydrogenation and dehydrogenation step facilitation, and selective influence on β-scission and polymerization reactions.

3.3.2.5. Effect of oxygen-doped biochar catalyst. The catalytic effect of BCO on overall product distribution, aliphatic and aromatic hydrocarbon selectivity, and carbon number range during the co-pyrolysis of WS and PFAD are shown in Fig. 8 **(a)** and Fig. 8 **(b)**. BCO had no significant effect on total hydrocarbon yield or aliphatic and aromatic hydrocarbon selectivity. The total amount of hydrocarbons, phenols, and acids decreased slightly, while total ketones, alcohols, and esters increased minimally. However, the selectivity for C5 hydrocarbons decreased (from 11.8 % to 8.4 %), while the selectivity for heavier hydrocarbons increased (from 3.5 % to 6.7 %). Adding oxygen functional groups to the biochar surface was expected to improve the selectivity and reactivity of the pyrolytic product. The FTIR and other characterizations revealed that either the added functional groups were not stable under the pyrolysis conditions, or the treatment did not introduce a significant amount of new functional groups. This may be either because oxalic acid was ineffective as a doping agent under the conditions used, or the pyrolysis process might decompose the functional groups.

3.3.3. Comparative performance analysis of biochar catalysts

Overall, the comparative analysis demonstrated that all catalysts (except BCO) significantly increased total hydrocarbon production when compared to non-catalytic co-pyrolysis, indicating their superior catalytic efficiency in promoting hydrocarbon formation, with BCB having the highest (86.8 %), followed by BCP, BCN, and BC. The highest selectivity for aromatic hydrocarbons (36.7 %) was observed with BCB, which showed its effectiveness in promoting aromatization, followed by BCP, BC, and BCN. Among the carbon numbers, non-catalytic co-pyrolysis produced the most gasoline range hydrocarbons (91 % selectivity), followed by BCB, BC, BCN, BCO, and BCO while BCP demonstrated the highest selectivity for diesel range hydrocarbons (29.5 %), followed by BCO, BCN, BCB, and BC.

On the other hand, non-catalytic co-pyrolysis produced a significant amount (30.0 %) of oxygenates (phenols, acids, furans, esters, ketones, alcohols), which were substantially decreased by all catalysts to 21.48 % by BCN, 20.9 % by BC, 18.95 % by BCP, and 16.31 % by BCB.

Thus, based on comparative performance analysis, BCB was found to be the most efficient catalyst, improving both the quality and quantity of hydrocarbon produced. Consequently, BCB was selected to further optimize bio-oil quality by assessing the influence of pyrolysis temperature and feedstock to catalyst ratio during WS and PFAD co-pyrolysis.

3.4. Optimization of catalytic co-pyrolysis of PFAD and WS over boron-doped biochar

The effect of the feed-to-catalyst ratio on pyrolytic products at different pyrolysis temperatures is shown in Fig. 9. Generally, the amount of aromatic hydrocarbon increased while the amount of aliphatic hydrocarbon decreased as the pyrolysis temperature rose from 550 to 750 °C. This indicates that the catalytic properties of BCB promoted ring formation and dehydrogenation reactions, which were facilitated by higher temperatures.

At a feedstock to catalyst ratio of 1:1, the hydrocarbon yields peaked at 650 °C (86.9 %), indicating the best possible interaction between BCB's catalytic sites and the feedstock. A significant increase in aromatic hydrocarbons (36.8 %) suggested that cyclization and dehydrogenation reactions were facilitated. The highest selectivity of aromatic hydrocarbons at this ratio was 50.4 % at 750 °C. The distribution of carbon numbers illustrated a preference for C5–C11 (gasoline-range) hydrocarbons (90.1 % selectivity) at lower temperature (550 °C), and C12-C20 (diesel range) at higher temperature (750 °C) with the 18.2 % selectivity.

The trend of rising hydrocarbon yield with temperature persisted when the feedstock to catalyst ratio was changed to 2:1, reaching a peak at 750 °C (90.8 %). The significant rise in aromatic selectivity (63.5 %) at this temperature highlighted the ability of BCB to stimulate aromatic condensation reactions at a lower catalyst loading. At 750 °C, the selectivity to C5–C11 remained high (74.2 %), while the ratio of C12–C20 (diesel-range hydrocarbons) increased in comparison to the 1:1 feedstock to catalyst ratio.

When the catalyst concentration was further diluted (4:1 ratio), a decrease in hydrocarbon yield was evident at 650 °C although it recovered at 750°C (70.9 %), highlighting a threshold in catalyst concentration for effective catalytic activity. Here, the aromatic selectivity was highest at 750 °C (53.3 %), demonstrating the influence of temperature on promoting ring formation. Furthermore, the selectivity towards C5-C11 hydrocarbons was found to be predominant at lower temperatures (82.1 % at 550 °C), which then decreased with increasing temperature, reaching 62.7 % at 750 °C.

Concurrently, the percentage of C12-C20 hydrocarbons decreased from 17.9 % at 550 °C to 17.3 % at 750 °C. The optimal conditions for co-pyrolysis of WS and PFAD over BCB catalyst were found to be a 2:1 feedstock-to-catalyst ratio and a temperature of 750 °C. Under these conditions, the hydrocarbon yield reached its highest level (90.8 %), with greater selectivity for aromatic hydrocarbons (63.5 %). The high

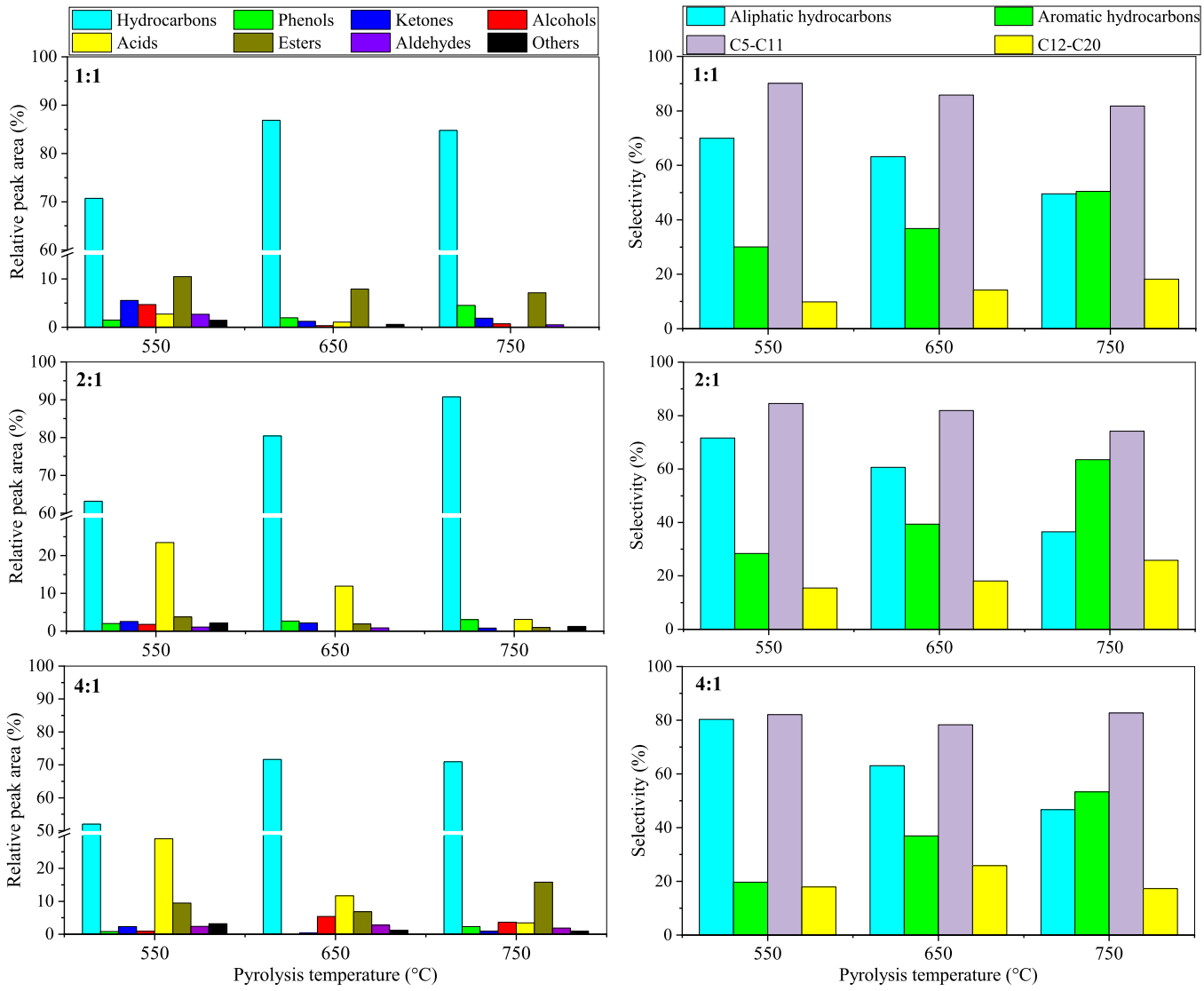

Fig. 9. Effect of pyrolysis temperature on overall product distribution and selectivity towards aliphatic and aromatic hydrocarbons and selectivity of carbon number ranges during the co-pyrolysis of WS and PFAD over a BCB catalyst for feedstock to catalyst ratios of 1:1, 2:1 and 4:1.

temperature and moderate catalyst concentration were also beneficial for diesel range hydrocarbons as evidenced by a 25.8 % selectivity towards C12-C20 hydrocarbons.

3.5. Role of BCB catalyst in co-pyrolysis of WS and PFAD

The possible role of BCB catalyst in the co-pyrolysis process of WS and PFAD can be explained based on the comprehensive investigations and detailed characterizations of feedstocks (WS and PFAD), BCB catalyst and the catalytic and non-catalytic pyrolytic products of WS and PFAD. As shown in Fig. 10, during co-pyrolysis, WS components (cellulose, hemicellulose, and lignin) undergo cracking (decarboxylation, decarbonylation and depolymerization), generating pyrolysis volatile intermediates. Simultaneously, PFAD components (palmitic acid, linoleic acid, stearic acid, and oleic acid) undergoing cracking via β-scission [62], which was catalyzed by the boron-doped active sites of BCB, producing intermediates such as aliphatics, fatty acid esters and lighter fractions. BCB's unique characteristics, such as its high surface area and well-developed pore structure, assisted in stabilizing and absorbing reactive intermediates. Boron sites promoted dehydration and decarboxylation reactions, which removed CO_2 and oxygen in the form of water while converting oxygenates into hydrocarbons. These catalytic sites also aided in aromatization via cyclization and hydrogen transfer processes. The aromatic rings in lignin in WS and fatty acid esters in PFAD emphasized a free radical mechanism in which free radicals generated from thermal cracking were stabilized and recombined. Aromatics were produced through Diels-Alder reactions, in which intermediate unsaturated compounds from WS and PFAD reacted to form cyclic structures that were then dehydrogenated into benzene, toluene, xylene, and other aromatic hydrocarbons [4]. Acidic boron sites on BCB boosted the hydrocarbon pool by converting long-chain hydrocarbons into smaller alkenes that then formed aromatic structures. This transformation was supported by its high selectivity for aromatic hydrocarbons, as evidenced by increased aromatic selectivity at 750 °C with a feedstock-to-catalyst ratio of 2:1.

Overall, BCB catalyzed a series of reactions that include deoxygenation, olefin synthesis, and cyclization, ultimately enriching the product with useful hydrocarbons while limiting oxygenated byproducts. The integrated approach emphasized the catalyst's critical role in increasing hydrocarbon yields, particularly aromatic species, by combining the intrinsic features of both feedstock types.

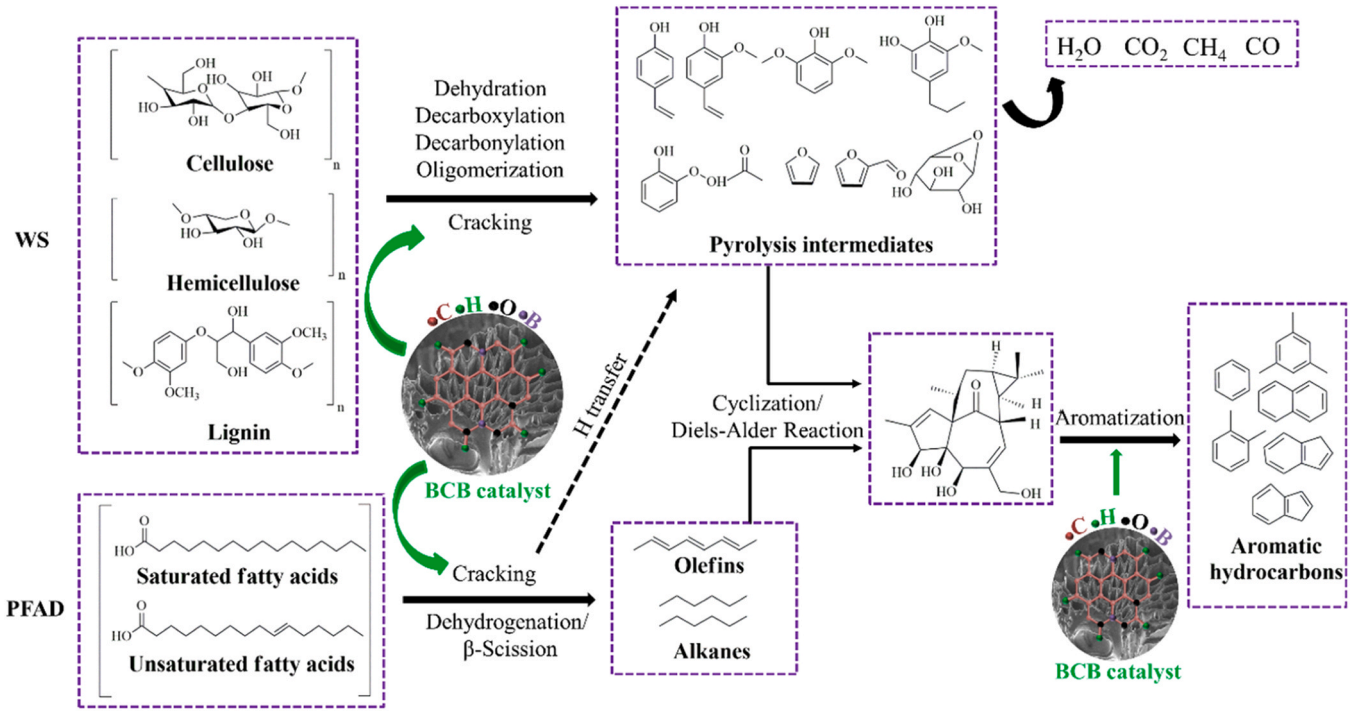

Fig. 10. The Possible pathways for catalytic co-pyrolysis of WS and PFAD over BCB catalyst.

4. Conclusions

The current study investigated the effects of nitrogen, phosphorus, oxygen, and boron doping on the catalytic properties of biochar produced from sugarcane bagasse (SCB) and their effectiveness for bio-oil upgrading in the co-pyrolysis of walnut shells (WS) and palm oil fatty acid distillate (PFAD) using Pyro/GC-MS. The findings showed that wet impregnation of SCB biomass with various precursors (boric acid, oxalic acid, urea, and phosphoric acid) followed by pyrolysis successfully introduced the targeted hetero atoms (B, O, N and P) in the resultant biochars, as evidenced by FTIR analysis, and induced certain changes in biochar's catalytic properties. The textural analysis revealed that the boric acid and oxalic acid treatments significantly increased the specific surface area and porosity of the biochars, whereas the urea and phosphoric acid treatments decreased surface and porosity when compared to pristine biochar which were consistent to the FE-SEM observations. The NH_3 TPD analysis revealed that boron-doped biochar had the highest desorption intensity, particularly at higher temperatures, indicating higher acidity. Comparative performance analysis of catalytic co-pyrolysis of WS and PFAD at 650 °C demonstrated that all catalysts (except BCO) significantly increased total hydrocarbon production when compared to non-catalytic co-pyrolysis, indicating their superior catalytic efficiency in promoting hydrocarbon formation, with BCB having the highest (86.8 %), followed by BCP, BCN, and BC. The highest selectivity for aromatic hydrocarbons (36.7 %) was observed with BCB, which showed its effectiveness in promoting aromatization, followed by BCP, BC, and BCN. The optimum process conditions and bio-oil quality were obtained over the BCB catalyst at a feedstock-to-catalyst ratio of 2:1 and a pyrolysis temperature of 750 °C, with a hydrocarbon yield of 90.8 % and aromatic hydrocarbon selectivity of 63.5 %.

Overall, this study emphasized the economic and environmental benefits of biochar catalysts derived from agricultural residues or waste biomass for bio-oil upgrading, and it is consistent with the principles of green chemistry and circular economy, aiming for waste valorization.

CRediT authorship contribution statement

Premchand: Writing – original draft, Validation, Methodology, Investigation, Data curation, Conceptualization, Writing – review & editing. **Elsa Antunes:** Writing – review & editing, Supervision, Resources, Project administration, Data curation, Conceptualization. **George O'Connell:** Writing – review & editing, Supervision, Formal analysis. **Jason Scott:** Writing – review & editing, Supervision, Formal analysis. **Samir Bensaid:** Writing – review & editing, Supervision. **David Chiaramonti:** Writing – review & editing, Supervision. **Debora Fino:** Writing – review & editing, Supervision, Project administration, Conceptualization. **Francesca Demichelis:** Writing – review & editing, Supervision, Data curation, Conceptualization.

Declaration of Competing Interest

The authors declare that they have no known competing financial interests or personal relationships that could have appeared to influence the work reported in this paper.

Data availability

Data will be made available on request.

Acknowledgments

This article and its related research work were conducted as part of the Italian inter-university PhD program in sustainable development and climate change (https://www.phd-sdc.it/).

Appendix A. Supporting information

Supplementary data associated with this article can be found in the online version at doi:10.1016/j.jece.2024.113630.

References

[1] P. Premchand, F. Demichelis, D. Chiaramonti, S. Bensaid, D. Fino, Biochar production from slow pyrolysis of biomass under CO_2 atmosphere: a review on the effect of CO_2 medium on biochar production, characterisation, and environmental applications, J. Environ. Chem. Eng. 11 (2023) 110009.

[2] A.K. Vuppaladadiyam, S.S.V. Vuppaladadiyam, A. Awasthi, A. Sahoo, S. Rehman, K.K. Pant, S. Murugavelh, Q. Huang, E. Anthony, P. Fennel, Biomass pyrolysis: a review on recent advancements and green hydrogen production, Bioresour. Technol. 364 (2022) 128087.

[3] N. Koralkar, P.K. Ghodke, Technical Criteria for Converting Biomass to High Liquid Bio-Oil Yields, in: Thermochemical and Catalytic Conversion Technologies for Future Biorefineries, Volume 1, Springer, 2022, pp. 189–203.

[4] T.T.K. Dada, M. Sheehan, S. Murugavelh, E. Antunes, A review on catalytic pyrolysis for high-quality bio-oil production from biomass, Biomass-.-. Convers. Biorefin. 13 (4) (2023) 2595–2614.

[5] R. French, S. Czernik, Catalytic pyrolysis of biomass for biofuels production, Fuel Process. Technol. 91 (1) (2010) 25–32.

[6] R. Venderbosch, A critical view on catalytic pyrolysis of biomass, ChemSusChem 8 (8) (2015) 1306–1316.

[7] Z. Qiu, Y. Zhai, S. Li, X. Liu, X. Liu, B. Wang, Y. Liu, C. Li, Y. Hu, Catalytic co-pyrolysis of sewage sludge and rice husk over biochar catalyst: bio-oil upgrading and catalytic mechanism, Waste Manag. 114 (2020) 225–233.

[8] S. Wang, H. Li, M. Wu, Advances in metal/biochar catalysts for biomass hydro-upgrading: a review, J. Clean. Prod. 303 (2021) 126825.

[9] J. Lee, K.-H. Kim, E.E. Kwon, Biochar as a catalyst, Renew. Sust. Energ. Rev. 77 (2017) 70–79.

[10] W. Chen, K. Li, M. Xia, H. Yang, Y. Chen, X. Chen, Q. Che, H. Chen, Catalytic deoxygenation co-pyrolysis of bamboo wastes and microalgae with biochar catalyst, Energy 157 (2018) 472–482.

[11] Q. Zhang, D. Zhang, H. Xu, W. Lu, X. Ren, H. Cai, H. Lei, E. Huo, Y. Zhao, M. Qian, X. Lin, Biochar filled high-density polyethylene composites with excellent properties: towards maximizing the utilization of agricultural wastes, Ind. Crops Prod. 146 (2020) 112185.

[12] M.Z. Yameen, H. AlMohamadi, S.R. Naqvi, T. Noor, W.-H. Chen, N.A.S. Amin, Advances in production & activation of marine macroalgae-derived biochar catalyst for sustainable biodiesel production, Fuel 337 (2023) 127215.

[13] C. Li, C. Zhang, M. Gholizadeh, X. Hu, Different reaction behaviours of light or heavy density polyethylene during the pyrolysis with biochar as the catalyst, J. Hazard. Mater. 399 (2020) 123075.

[14] A. Al-Rumaihi, M. Shahbaz, G. Mckay, H. Mackey, T. Al-Ansari, A review of pyrolysis technologies and feedstock: a blending approach for plastic and biomass towards optimum biochar yield, Renew. Sust. Energ. Rev. 167 (2022) 112715.

[15] R. Zou, C. Wang, M. Qian, E. Huo, X. Kong, Y. Wang, L. Dai, L. Wang, X. Zhang, W. C. Mateo, Catalytic co-pyrolysis of solid wastes (low-density polyethylene and lignocellulosic biomass) over microwave assisted biochar for bio-oil upgrading and hydrogen production, J. Clean. Prod. 374 (2022) 133971.

[16] L. Zhu, Y. Zhang, H. Lei, X. Zhang, L. Wang, Q. Bu, Y. Wei, Production of hydrocarbons from biomass-derived biochar assisted microwave catalytic pyrolysis, Sustain. Energy Fuels 2 (8) (2018) 1781–1790.

[17] S. Liu, G. Wu, Y. Gao, B. Li, Y. Feng, J. Zhou, X. Hu, Y. Huang, S. Zhang, H.J.R. E. Zhang, Understanding the catalytic upgrading of bio-oil from pine pyrolysis over CO_2-activated biochar, Renew. Energy 174 (2021) 538–546.

[18] J. Du, T. Shen, J. Hu, F. Zhang, S. Yang, H. Liu, H.J.E. Wang, Study on thermochemical conversion of triglyceride biomass catalyzed by biochar catalyst, Energy 277 (2023) 127733.

[19] P. Maneechakr, S.J.Ao Karnjanakom, Improving the bio-oil quality via effective pyrolysis/deoxygenation of palm kernel cake over a metal (Cu, Ni, or Fe)-doped carbon catalyst, ACS Omega 6 (30) (2021) 20006–20014.

[20] S. Liu, G. Wu, S.S.A. Syed-Hassan, B. Li, X. Hu, J. Zhou, Y. Huang, S. Zhang, H.J. F. Zhang, Catalytic pyrolysis of pine wood over char-supported Fe: Bio-oil upgrading and catalyst regeneration by CO_2/H_2O, Fuel 307 (2022) 121778.

[21] C. Yuan, A.E.-F. Abomohra, S. Wang, Q. Liu, S. Zhao, B. Cao, X. Hu, F. Marrakchi, Z. He, Y.J.J.O.C.P. Hu, High-grade biofuel production from catalytic pyrolysis of waste clay oil using modified activated seaweed carbon-based catalyst, J. Clean. Prod. 313 (2021) 127928.

[22] R. Xu, C. Yan, Q. Liu, E. Liu, H. Zhang, X. Zhang, X. Yuan, L. Han, H. Lei, R. Ruan, Development of metal-doping mesoporous biochar catalyst for co-valorizing biomass and plastic waste into valuable hydrocarbons, syngas, and carbons, Fuel Process. Technol. 227 (2022) 107127.

[23] W. Luo, T. Wang, S. Zhang, D. Zhang, H. Dong, M. Song, Z. Zhou, Catalytic co-pyrolysis of herb residue and polypropylene for pyrolysis products upgrading and diversification using nickel-X/biochar and ZSM-5 (X= iron, cobalt, copper), Bioresour. Technol. 349 (2022) 126845.

[24] C.-M. Hung, C.-W. Chen, C.-P. Huang, C.-D. Dong, Metal-free single heteroatom (N, O, and B)-doped coconut-shell biochar for enhancing the degradation of sulfathiazole antibiotics by peroxymonosulfate and its effects on bacterial community dynamics, Environ. Pollut. 311 (2022) 119984.

[25] H. Lyu, J.Y. Lim, Q. Zhang, S. Senadheera, C. Zhang, Q. Huang, Y.S. Ok, Conversion of organic solid waste into energy and functional materials using biochar catalyst: bibliometric analysis, research progress, and directions, Appl. Catal. B: Environ. (2023) 123223.

[26] W. Chen, Y. Fang, K. Li, Z. Chen, M. Xia, M. Gong, Y. Chen, H. Yang, X. Tu, H. Chen, Bamboo wastes catalytic pyrolysis with N-doped biochar catalyst for phenols products, Appl. Energy 260 (2020) 114242.

[27] D. Duan, Y. Zhang, H. Lei, E. Villota, R. Ruan, Renewable jet-fuel range hydrocarbons production from co-pyrolysis of lignin and soapstock with the activated carbon catalyst, Waste Manag. 88 (2019) 1–9.

[28] Z. Su, K. Jin, J. Wu, P. Huang, L. Liu, Z. Xiao, H. Peng, L. Fan, W. Zhou, Phosphorus doped biochar as a deoxygenation and denitrogenation catalyst for ex-situ upgrading of vapors from microwave-assisted co-pyrolysis of microalgae and waste cooking oil, J. Anal. Appl. Pyrolysis 164 (2022) 105538.

[29] S. Annamalai, W.S. Shin, Algae-derived metal-free boron-doped biochar acts as a catalyst for the activation of peroxymonosulfate toward the degradation of diclofenac, Environ. Pollut. 331 (2023) 121850.

[30] K.O. Iwuozor, E.C. Emenike, J.O. Ighalo, F.O. Omoarukhe, P.E. Omuku, A. G. Adeniyi, Review on the thermochemical conversion of sugarcane bagasse into biochar, Clean. Mater. (2022) 100162.

[31] S. Fordos, N. Abid, M. Gulzar, I. Pasha, F. Oz, A. Shahid, M.K.I. Khan, A. Mousavi Khaneghah, R.M. Aadil, Recent development in the application of walnut processing by-products (walnut shell and walnut husk), Biomass-.-. Convers. Biorefin. 13 (16) (2023) 14389–14411.

[32] J.E. Lam, A.R. Mohamed, A.N.K. Lup, M.K. Koh, Palm fatty acid distillate derived biofuels via deoxygenation: properties, catalysts and processes, Fuel Process. Technol. 236 (2022) 107394.

[33] Y. Cheng, J. Yang, J. Shen, P. Yan, S. Liu, J. Kang, L. Bi, B. Wang, S. Zhao, Z. Chen, Preparation of P-doped biochar and its high-efficient removal of sulfamethoxazole from water: adsorption mechanism, fixed-bed column and DFT study, Chem. Eng. J. 468 (2023) 143748.

[34] H. Wang, W. Guo, B. Liu, Q. Wu, H. Luo, Q. Zhao, Q. Si, F. Sseguya, N. Ren, Edge-nitrogenated biochar for efficient peroxydisulfate activation: an electron transfer mechanism, Water Res 160 (2019) 405–414.

[35] L. Zhang, L. Huang, S. Li, X. Zhu, Study on two-step pyrolysis of walnut shell coupled with acid washing pretreatment, J. Anal. Appl. Pyrolysis 136 (2018) 1–7.

[36] T.K. Dada, A. Vuppaladadiyam, A.X. Duan, R. Kumar, E. Antunes, Probing the effect of Cu-SrO loading on catalyst supports (ZSM-5, Y-zeolite, activated carbon, Al_2O_3, and ZrO_2) for aromatics production during catalytic co-pyrolysis of biomass and waste cooking oil, Bioresour. Technol. 360 (2022) 127515.

[37] D. Chen, K. Cen, X. Zhuang, Z. Gan, J. Zhou, Y. Zhang, H. Zhang, Insight into biomass pyrolysis mechanism based on cellulose, hemicellulose, and lignin: Evolution of volatiles and kinetics, elucidation of reaction pathways, and characterization of gas, biochar and bio-oil, Combust. Flame 242 (2022) 112142.

[38] J. Nisar, N. Khan, G. Ali, F. Muhammad, A. Shah, A. Sharif, E. Ahmed, Thermo-catalytic decomposition of walnut shells waste over cobalt doped cerium oxide: Impact of catalyst on kinetic parameters and composition of bio-oil, Chem. Eng. Sci. 282 (2023) 119355.

[39] A.G.H. Saif, S.S. Wahid, M.R. Ali, Pyrolysis of sugarcane bagasse: the effects of process parameters on the product yields, Mater. Sci. Forum, Trans. Tech. Publ. (2020) 159–167.

[40] K. Kameyama, T. Miyamoto, Y. Iwata, The preliminary study of water-retention related properties of biochar produced from various feedstock at different pyrolysis temperatures, Materials 12 (11) (2019) 1732.

[41] Z. Sun, D. Yao, H. Guo, H. Zhu, W. Hua, Q. Yuan, L. Zhang, Q. Fan, B. Yi, Catalytic mechanism of N-containing biochar on volatile-biochar interaction for the same origin pyrolysis, J. Environ. Manag. 336 (2023) 117710.

[42] Z. Li, B. Xing, Y. Ding, Y. Li, S. Wang, A high-performance biochar produced from bamboo pyrolysis with in-situ nitrogen doping and activation for adsorption of phenol and methylene blue, Chin. J. Chem. Eng. 28 (11) (2020) 2872–2880.

[43] M. Zhou, Y. Xu, G. Luo, Q. Zhang, L. Du, X. Cui, Z. Li, Facile synthesis of phosphorus-doped porous biochars for efficient removal of elemental mercury from coal combustion flue gas, Chem. Eng. J. 432 (2022) 134440.

[44] A. Ateş, B. Aydemir, K.E. Öksüz, Investigation of physicochemical and biological properties of boron-doped biochar, Biomass-.-. Convers. Biorefin. (2023) 1–15.

[45] B. Liu, W. Guo, H. Wang, Q. Si, Q. Zhao, H. Luo, N. Ren, B-doped graphitic porous biochar with enhanced surface affinity and electron transfer for efficient peroxydisulfate activation, Chem. Eng. J. 396 (2020) 125119.

[46] X. Wang, Y. Liu, L. Zhu, Y. Li, K. Wang, K. Qiu, N. Tippayawong, P. Aggarangsi, P. Reubroycharoen, S. Wang, Biomass derived N-doped biochar as efficient catalyst supports for CO_2 methanation, J. CO_2 Util. 34 (2019) 733–741.

[47] H. Yang, P. Chen, W. Chen, K. Li, M. Xia, H. Xiao, X. Chen, Y. Chen, X. Wang, H. Chen, Insight into the formation mechanism of N, P co-doped mesoporous biochar from H_3PO_4 activation and NH_3 modification of biomass, Fuel Process. Technol. 230 (2022) 107215.

[48] P. Premchand, F. Demichelis, D. Chiaramonti, S. Bensaid, D. Fino, Study on the effects of carbon dioxide atmosphere on the production of biochar derived from slow pyrolysis of organic agro-urban waste, Waste Manag. 172 (2023) 308–319.

[49] M. Premchand, Aqsha Komiyama, Y. Uemura, A comparative study of oil palm fronds torrefaction under flue gas and nitrogen atmospheres, J. Oil Palm. Res. 35 (1) (2022) 75–85.

[50] Q. Zhou, X. Jiang, X. Li, C. Jia, W. Jiang, Preparation of high-yield N-doped biochar from nitrogen-containing phosphate and its effective adsorption for toluene, RSC Adv. 8 (53) (2018) 30171–30179.

[51] N. Kasera, S. Hall, P. Kolar, Effect of surface modification by nitrogen-containing chemicals on morphology and surface characteristics of N-doped pine bark biochars, J. Environ. Chem. Eng. 9 (2) (2021) 105161.

[52] S.S. Qureshi, Premchand, M. Javed, S. Saeed, R. Abro, S.A. Mazari, N.M. Mubarak, M.T.H. Siddiqui, H.A. Baloch, S. Nizamuddin, Hydrothermal carbonization of oil palm trunk via taguchi method, Korean J. Chem. Eng. 38 (2021) 797–806.

[53] J. Pan, H. Deng, Z. Du, K. Tian, J. Zhang, Design of nitrogen-phosphorus-doped biochar and its lead adsorption performance, Environ. Sci. Pollut. Res. 29 (2022) 1–11.

[54] L. Sui, C. Tang, Q. Du, Y. Zhao, K. Cheng, F. Yang, Preparation and characterization of boron-doped corn straw biochar: Fe (II) removal equilibrium and kinetics, J. Environ. Sci. 106 (2021) 116–123.
[55] J. Berlin, Analysis of boron with energy dispersive x-ray spectrometry, Imaging Microsc. 13 (2011) 19–21.
[56] Y. Kar, Co-pyrolysis of walnut shell and tar sand in a fixed-bed reactor, Bioresour. Technol. 102 (20) (2011) 9800–9805.
[57] M.A. Shah, N. Khan, V. Kumar, A. Qurashi, Pyrolysis of walnut shell residues in a fixed bed reactor: Effects of process parameters, chemical and functional properties of bio-oil, J. Environ. Chem. Eng. 9 (4) (2021) 105564.
[58] T. Kan, V. Strezov, T.J. Evans, Lignocellulosic biomass pyrolysis: a review of product properties and effects of pyrolysis parameters, Renew. Sust. Energ. Rev. 57 (2016) 1126–1140.
[59] S.-J. Oh, G.-G. Choi, J.-S. Kim, Production of acetic acid-rich bio-oils from the fast pyrolysis of biomass and synthesis of calcium magnesium acetate deicer, J. Anal. Appl. Pyrolysis 124 (2017) 122–129.
[60] J. Asomaning, P. Mussone, D.C. Bressler, Pyrolysis of polyunsaturated fatty acids, Fuel Process. Technol. 120 (2014) 89–95.
[61] Y. Qiao, B. Wang, P. Zong, Y. Tian, F. Xu, D. Li, F. Li, Y. Tian, Thermal behavior, kinetics and fast pyrolysis characteristics of palm oil: analytical TG-FTIR and Py-GC/MS study, Energy Convers, Manag 199 (2019) 111964.
[62] A.K. Tripathi, D.K. Ojha, R. Vinu, Selective production of valuable hydrocarbons from waste motorbike engine oils via catalytic fast pyrolysis using zeolites, J. Anal. Appl. Pyrolysis 114 (2015) 281–292.
[63] J. Asomaning, P. Mussone, D.C. Bressler, Thermal deoxygenation and pyrolysis of oleic acid, J. Anal. Appl. Pyrolysis 105 (2014) 1–7.
[64] D. Jiang, C. Yuan, X. Cheng, S. Wang, H. Li, X. Yang, Study on the pyrolysis mechanism of unsaturated fatty acid: a combined density functional theory and experimental study, Int. J. Energy Res. 46 (2) (2022) 2029–2040.
[65] G. Chang, P. Miao, H. Wang, L. Wang, X. Hu, Q. Guo, A synergistic effect during the co-pyrolysis of Nannochloropsis sp. and palm kernel shell for aromatic hydrocarbon production, Energy Convers. Manag. 173 (2018) 545–554.
[66] Y. Zhang, H. Lei, Z. Yang, D. Duan, E. Villota, R. Ruan, From glucose-based carbohydrates to phenol-rich bio-oils integrated with syngas production via catalytic pyrolysis over an activated carbon catalyst, Green. Chem. 20 (14) (2018) 3346–3358.
[67] X. Lin, X. Chen, P. Fu, B. Tang, D. Bi, Highly efficient production of monocyclic aromatics from catalytic co-pyrolysis of biomass and plastic with nitrogen-doped activated carbon catalyst, Chem. Eng. J. 474 (2023) 145783.
[68] P. Li, K. Wan, H. Chen, F. Zheng, Z. Zhang, B. Niu, Y. Zhang, D. Long, Value-added products from catalytic pyrolysis of lignocellulosic biomass and waste plastics over biochar-based catalyst: a state-of-the-art review, Catalysts 12 (9) (2022) 1067.